GA–A23261

DOUBLE-NULL DIVERTOR DESIGN FOR JT–60SU, A 10 Mamp CLASS LONG-PULSE TOKAMAK

by
W.P. WEST, C.B. BAXI, M.E. FRIEND, D.A. HUMPHREYS,
J.A. LEUER, T.W. PETRIE, E.E. REIS, S. ISHIDA,
G. KURITA, Y. NEYATANI, A. SAKASAI

OCTOBER 1999

DISCLAIMER

This report was prepared as an account of work sponsored by an agency of the United States Government. Neither the United States Government nor any agency thereof, nor any of their employees, makes any warranty, express or implied, or assumes any legal liability or responsibility for the accuracy, completeness, or usefulness of any information, apparatus, product, or process disclosed, or represents that its use would not infringe privately owned rights. Reference herein to any specific commercial product, process, or service by trade name, trademark, manufacturer, or otherwise, does not necessarily constitute or imply its endorsement, recommendation, or favoring by the United States Government or any agency thereof. The views and opinions of authors expressed herein do not necessarily state or reflect those of the United States Government or any agency thereof.

GA–A23261

DOUBLE-NULL DIVERTOR DESIGN FOR JT–60SU, A 10 Mamp CLASS LONG-PULSE TOKAMAK

by
W.P. WEST, C.B. BAXI, M.E. FRIEND, D.A. HUMPHREYS, J.A. LEUER,
T.W. PETRIE, E.E. REIS, S. ISHIDA,* G. KURITA,*
Y. NEYATANI,* A. SAKASAI*

This is a preprint of a paper to be submitted
for publication in *Fusion Technology.*

*Japan Atomic Energy Research Institute,
Naka-machi, Naka-gun, Ibaraki-ken, Japan

GA PROJECT 04945
OCTOBER 1999

ABSTRACT

This paper presents the design of a double-null divertor for use in JT–60SU. The free boundary equilibrium code EFIT is used to establish a symmetric highly triangular double-null plasma shape. The baffle shapes are highly contoured to match the equilibrium, with the plasma-facing surfaces intersecting the flux surfaces at steep angles in the regions of high heat flux. These contoured surfaces also provide a tightly baffled design with small aperture pumping gaps near both the inner and outer divertor strike points. The gaps provide adequate throughput of D_2 gas for active control of impurity entrainment at reasonable pressures. The structural design is shown to be consistent with both forces from disruptions and thermal stress during vacuum vessel bakeout.

1. INTRODUCTION

JT–60SU is a design study for a superconducting, long-pulse upgrade to the existing JT–60U tokamak. The basic design of the JT–60SU advanced tokamak allows operation in a true double-null (DN) diverted configuration. In this paper, a JT–60SU divertor design is presented to accommodate DN operation. This divertor design is consistent with a highly triangular DN shape that was obtained using the EFIT-free boundary equilibrium solver [1]. The baffle shapes in this design are highly contoured with the plasma-facing surfaces intersecting the flux surfaces at steep angles in the regions of high heat flux. These contoured surfaces also provide a tightly baffled design with pumping gaps near both the inner and outer divertor strike points. The gaps provide adequate throughput of D_2 gas for active control of impurity entrainment at reasonable pressures.

The DN shape is of interest in JT–60SU because devices like DIII–D have demonstrated higher performance compared to similar single–null (SN) configurations. In the DN configuration, the shape can have high triangularity both upper and lower. The higher triangularity allows higher beta plasmas through increased plasma current for the same edge safety factor, q_{95}. This higher performance can result not only in higher equivalent fusion power, but also in higher bootstrap current fractions.

The design presented here, Fig. 1, is up/down symmetric. It is our opinion that symmetry in the design is highly desirable for several reasons:

- A reduction of the peak heat load at the outer strike points is achievable in balanced DN.
- A symmetric baffling and pumping design is needed to balance the particle flux and pumping capability.
- Vertical position control with the pf coil set cannot assure that either divertor will not become the dominant divertor and receive all the outflux of particles and heat.
- Loss of vertical control during disruptions is minimized when operating at the neutral point [2,3] and a symmetric DN assures operation at the neutral point.

We also avoid the use of insulators on structural elements, since unforeseen degradation of voltage hold-off capability can lead to large-current arcs and unanticipated large forces. We prefer, instead, to provide clear grounding paths and designs capable of withstanding the expected forces. Thus, the supporting structures must be flexible enough to relax under the displacements expected during bakeout of the vacuum vessel, yet stiff enough to resist the loads due to halo currents.

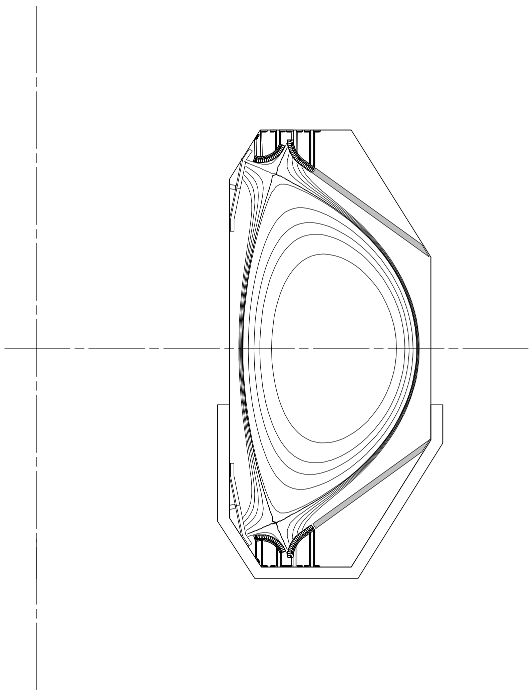

Fig. 1. A cross section of the DN baffles in JT–60SU along with the flux surfaces from the EFIT equilibrium. The baffles are up/down symmetric.

In this report, we will briefly review the equilibrium analysis using the EFIT code to develop the DN configuration. The contoured baffle geometry compatible with this shape will be shown. A study of the expected heat loads on the baffle surfaces will be presented, and a thermal analysis of a proposed actively cooled copper block with a brazed graphite tile surface will be presented. Conceptual designs of the baffle plates using this actively cooled tile geometry will be presented. A detailed analysis of expected halo currents during vertical displacement events (VDE) will be presented. A design of the supporting structure will be shown, and an analysis of the loads on particular members during bakeout and VDEs will be presented. It will be shown that these loads are consistent with the design if Inconel 718 is used for the vertical supporting members. A rough estimate of the conductance of the gaps in the divertor for D_2 gas will be presented and shown to be consistent with the D_2 throughput required for active control of impurities using the puff and pump technique.

The design presented here is intended for use during the deuterium phase of operation of JT–60SU. The radiation and plasma materials interaction effects accompanying operation with significant amounts of tritium have not been considered in this design. Such effects as tritium uptake by plasma-facing graphite surfaces and neutron activation of structural supports would likely influence the design of the divertor significantly. This divertor design would provide a long period for gaining operating experience and provide an experimental database for designing a DT tolerant divertor.

2. PLASMA EQUILIBRIUM AND DIVERTOR SHAPE

A 10 MA DN equilibrium for JT–60SU has been developed using the EFIT equilibrium [1] solver. Some of the global shape parameters are given in Table 1. Internal profiles of current and pressure, consistent with the global parameters given in Table 1, are not shown. The equilibrium is defined at the approximate start-of-flattop (SOF) fiducial state, which was established based on approximating the initial magnetization state and subtracting flux associated with break down and resistive losses. The SOF state is typically the most critical flux state for the divertor coils. Results indicate that if the amp-turn capability of the lower pf coils that define the divertor, as presently designed for JT–60SU [4,5], is used on the upper divertor coils then the coil system should be approximately capable of producing the 10 MA DN equilibrium. However, only a single shape and β_p, ℓ_i point has been checked.

TABLE 1
GLOBAL SHAPE PARAMETERS FOR THE 10 MA, 6.25 T SYMMETRIC DOUBLE-NULL EFIT EQUILIBRIUM

R_m	=	5.16 m
a	=	1.49 m
κ	=	2.10
δ	=	0.63
q_{95}	=	3.8
ℓ_i	=	1.04
β_p	=	0.75
β_t	=	1.62%
W_{dia}	=	200 MJ

To be complete, the flux at the end of burn (EOB) fiducial state was estimated based on an assumed current limit of 19 MA-turns in each of the four central coils that make up the central solenoid [4,5]. The shape and plasma parameters are almost identical to the SOF state.

The intent of this study is to provide a design for a tightly baffled divertor with pumping on both legs. Such a design requires detailed knowledge of the flux surfaces in the divertor region, and the above equilibrium provides these required details. This study was limited to a single β_p and ℓ_i operating point. More extensive studies of variations in operating conditions (*e.g.*, β_p and ℓ_i) on the divertor flux surfaces, and investigations of the ability of the pf coil and power supply set to control the divertor strike point locations will be conducted in the future.

2.1. SHAPE OF DIVERTOR BAFFLES

The SOF equilibrium was used in designing the shapes of the divertor baffles. The baffle shapes were defined based on the need to provide tight baffling, to provide adequate pumping to allow active control of particle flow using the puff and pump technique, and to reduce the peak heat flux by contouring the baffle surfaces in the region of the outer strike point.

The structure is up/down symmetric. Because potential control system problems and plasma instabilities may lead to transient or long duration high heat fluxes or mechanical loads on either divertor, we feel that symmetry is required. We also feel that when operating in a DN configuration, particle control is optimized with symmetric pumping capability.

The DN divertor shape we propose is shown in Fig. 1 along with flux surfaces from the EFIT equilibrium. An enlargement of the lower divertor region is shown in Fig. 2. The baffles and support structures are up/down symmetric. The contoured surfaces of the outer baffle and the private baffle provide tight baffling. The flux surfaces outside the separatrix in these figures are the 1, 2, 3, and 4 cm surfaces measured at the midplane. The region near the outer strike point, where the heat and particle flux can achieve quite high values in standard attached divertor operation, is deeply confined within the narrow gap between the outer and private baffles and intersects the outer baffle at a steep angle. As discussed in Section 4.1, this steep angle of intersection provides a significant reduction in the peak surface heat flux predicted for JT–60SU and gives reasonable confidence in the active cooling design. The inner strike plate is designed to give some flexibility in the height of the X–point. At reduced plasma current, the pf coil set is capable of establishing equilibria with significantly higher X–points than

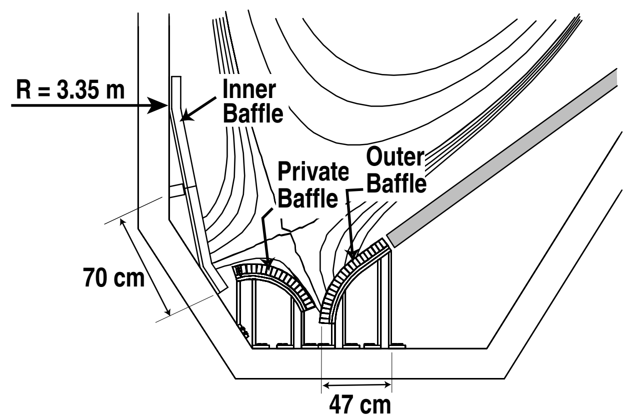

Fig. 2. A cross section of shape and vertical supports for the divertor baffles is shown in the JT–60SU vacuum vessel, along with a flux plot from the 44010.01020 EFIT DN equilibrium. The flux surfaces shown outside of the separatrix are the 1, 2, 3, and 4 cm surfaces measured at the midplane.

shown in these figures. The flat design of the inner plate will accommodate the motion of the strike zone as the X–point height is increased.

The gaps between the baffles, both inner and outer gaps, are designed to give reasonable conductance for D_2 gas as discussed in more detail in Section 5. The outer gap is positioned such that the separatrix can be placed on the outer baffle above the gap, deeply into the gap, or on the outer edge of the private baffle. The active cooling is designed to allow high heat flux in all these regions. The gap between the lowest extent of the outer baffle and vacuum vessel is large compared to the gap between the baffles and, therefore, has a comparably higher conductance.

To predict the recycling and neutral baffling performance of a divertor geometry requires extensive modeling using detailed 2–D fluid and Monte Carlo codes which is beyond the scope of this effort. However, experience from today's tokamaks, including JT–60U, ASDEX–Upgrade, JET, and DIII–D, shows that similar baffling configurations lead to improved trapping of neutrals in the divertor region. Such trapping has been shown to reduce the backflow of neutrals to the core plasma and to increase the window of operation in a detached divertor mode [6].

3. DIVERTOR MECHANICAL DESIGN

3.1. SUPPORT STRUCTURE CONCEPT

Basic geometry and a support system were developed based on the stresses expected due to halo currents and the thermal expansion during bakeout. Consideration was given to remote handling and maintenance. Simple component mounting schemes and supports were investigated. The divertor structure is presented in Fig. 2. As shown in this figure, the major components of the divertor are the outer baffle, the private flux baffle, the inner baffle, and their corresponding supports. The three baffles and their supporting structures are handled independently. Toroidally, each of the three baffle elements is divided into 45 equal segments, each 8° of arc. Each baffle segment is intended to be installed and maintained individually. A few of the major dimensions of the divertor components are also illustrated in Fig. 2. Sliding interfaces are avoided due to concerns of galling and self-welding. These two effects can result in unpredictable and undesirable movement and stresses in the components. The use of insulators is also avoided in this design. Both mechanical loads and voltages present during off-normal events can result in insulator failure and in unexpectedly large electromechanical forces on structural elements. Instead, clear grounding paths are provided and support structures are designed to take the loads predicted by well-validated models of tokamak disruptions (see Sections 3.2 and 3.3).

The details of the support concept are illustrated for the private and outer baffles in Fig. 3. Each 8° private baffle segment uses a 2.5 cm thick 316 LN stainless steel mounting plate as a base. This mounting plate is supported at its toroidal edges via a 2.5-cm thick, 316 LN stainless steel, splice plate that it shares with the adjacent private baffle components. Figure 3 shows the private baffle component being attached to the splice plate utilizing two rows of bolts. This shared support/splice plate arrangement effectively configures the baffle into one toroidally continuous ring. Each splice plate is then attached to the vacuum vessel by means of a pair of flexible twin plate supports. The splice plates and vertical supports are not designed for routine removal by remote handling equipment. Each support is 1.9 cm thick by 20.3 cm wide and is made of Inconel 718. The toroidal width of the baffle segments is about 60 cm, so the supports occupy

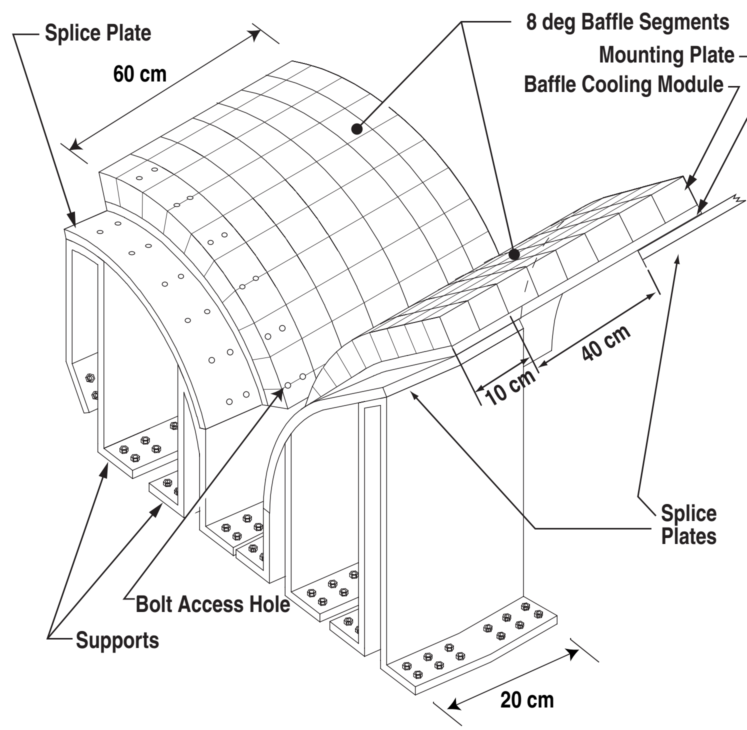

Fig. 3. 3–D representation of one section of the divertor showing the baffle segments, the vertical supports, and the splice plates. Adjacent divertor baffle segments share a splice plate.

only about one-third of the available space toroidally, leaving sufficient gaps for gas throughput requirements (see Section 5). The sizing of the supports will be discussed in Section 3.3 of this report. Inconel 718 is chosen over 316 LN for the vertical supports due to the far superior allowable stress (1035 MPa as compared to 410 MPa for thermal bakeout loads). Though Inconel has one-half the activation life of 316 LN (10 dpa as compared to 20 dpa for 316 LN), it is being proposed to be used during the D–D phase of operations. Furthermore, since it is only being used for the divertor supports, it will experience only half the neutron loading of material at the midplane (based on ITER data) and it is located underneath the baffle modules which will act to even further reduce neutron loading.

The design for the inner baffle supports is only presented as a preliminary concept in this paper. It is proposed that the lower end of the inner baffle be bolted directly to the vacuum vessel wall. The upper end of the baffle would be attached using short flexible supports.

Although no detailed remote maintenance design work has been completed, consideration for ease of use of remote maintenance equipment is given in both the segmentation of the baffle modules and the design of the component mounting system (Fig. 3). The split lines for both the inner and outer baffles are chosen so as to include the regions of high heat flux and be of a size consistent with removal through the midplane port. Though it would be desirable to have a nonspecific removal order for the divertor components, the geometry of the divertor dictates a set order. We make the following assumptions: (1) the remote manipulator has only rather simplified movements, (2) the location of the splits for the private baffle cooling tubes are underneath the private baffle, (3) remote pipe welder/cutter access is assumed to be available from the radially outboard direction, and (4) access to the bolts that attach the water-cooled modules to the splice plates is available from the plasma-facing side of the modules. With these assumptions, the private baffle has to be removed first. If bolt access is acceptable on the back side of the outer baffle, then the outer baffle and private baffle can be removed independently of each other. The inner baffle is effectively trapped until the private baffle is removed.

3.2. DISRUPTION HALO CURRENTS IN JT–60SU

Disrupting tokamak plasmas can produce large halo currents flowing on open field lines surrounding the core plasma, potentially applying extremely large localized stresses [7–9]. Halo currents in the divertor components are particularly large in disruptions resulting from VDEs. The present analysis includes effects demonstrated to be important in disruptions in DIII–D, JT–60U, and Alcator C–Mod [10–12]. Peak halo current amplitude is determined by machine geometry, vertical instability growth rate, and post-thermal quench core and halo plasma resistivities. In order to estimate the range of halo currents expected in JT–60SU due to vertical displacement events, the core and halo plasma resistivities are varied in a scoping study across a range suggested by device experience and ITER design assumptions [13].

Table 2 summarizes the assumptions used in the scoping study. Core and halo temperatures are taken to be equal, and this common temperature value is varied from 5 to 25 eV. The Z_{eff} of both core and halo are fixed at 1.5 and the vertical growth rate is fixed at the worst-case (largest) value expected to occur in JT–60SU (50 s^{-1}) [14].

TABLE 2
SUMMARY OF ASSUMPTIONS USED IN JT–60SU HALO CURRENT SCOPING STUDY

Assumption	Range of Value	Jusification
Post-thermal quench electron temperature $T_{e(core)} = T_{e(halo)}$	$5 \rightarrow 25$ eV	Worst-case assumption; Observed in experiment; Range corresponds to ITER fiducial range
Post-thermal quench $Z_{eff(core)} = Z_{eff(halo)}$	1.5	Simplicity; post-TQ Z_{eff} = 1.5 measured in DIII–D
Fixed vertical growth rate γ_{z0}	50 s^{-1}	= Highest γ_{z0} expected in JT–60SU; worst-case assumption
Fixed plasma current I_p	10 MA	Worst-case assumption

Figure 4 summarizes the results of the scoping study. The figure shows the peak poloidal halo current as a function of electron temperature (of both core and halo). The dashed line indicates the peak halo current in the case for which strong MHD is effectively turned on when the edge safety factor, q_e, reaches unity. The solid line shows the result of ignoring this effect. Accounting properly for the onset of this MHD requires further increase of the resistivity so that the core plasma current decays rapidly, causing the edge safety factor to rise. This phenomenon has been observed in both DIII–D and Alcator C–Mod VDEs and serves to limit the peak halo current for T_d > 17 eV. In this case, the study shows that the largest value of peak halo current expected in JT–60SU is 4.7 MA (with I_p = 10 MA, corresponding to a halo current fraction of $I_{h(pol)}/I_p$ = 0.47).

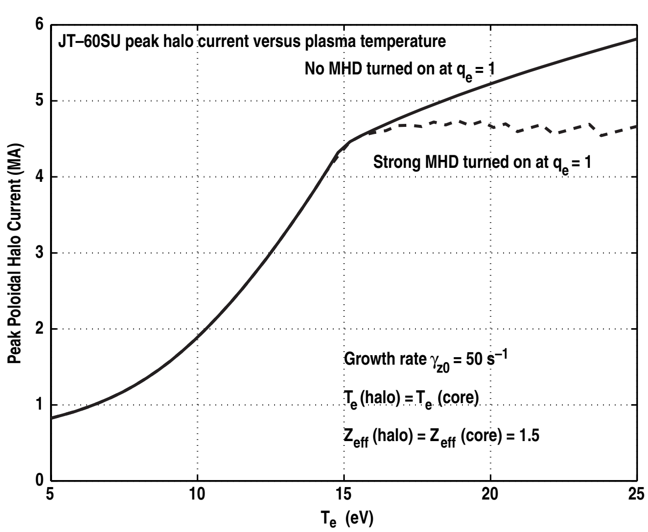

Fig. 4. Simulations of JT–60SU VDEs using γ_z = 50 s^{-1} show maximum poloidal halo current of $I_{h(pol)}$ = 4.7 MA ($I_{h(pol)}/I_p$ = 0.47).

The halo currents calculated in the present study were based on a worst-case growth rate derived from a study of LSN plasmas [14]. The growth rates for DN plasmas are not expected to be substantially different. In the worst case VDE events, any upper divertor hardware must be designed to handle the same forces as the lower divertor since VDE plasma motion is equally likely to be upward or downward. In a balanced DN, with operation at the neutral point, the frequency of disruption events leading to strong vertical motion will be substantially less than for SN operation.

3.3. JT–60SU DIVERTOR SUPPORT STRUCTURE STRESS ANALYSIS

The sizing calculations for the supports were performed for the poloidal flux baffle structure. At the toroidal ends of each 8° segment, the baffle is supported by plates of vertical height 27.0 cm at its inner radius and 25.2 cm at the outer radius. The peak loading conditions on the divertor structures occur during two distinct operating conditions and provide opposing criteria to the design. The halo current forces, discussed in the previous section, must be reacted by the support structure. Thus, a stiff support system is required. However, during conditioning of the vacuum vessel prior to plasma operations, the vessel is heated from room temperature to a peak value of 400°C. During this heating process, the vacuum vessel rises in temperature at a different rate than the divertor components and stresses due to differential thermal expansion occurs. This condition requires a level of flexibility to the support structure. The dome structure and the vacuum vessel are to be fabricated from 316 LN stainless steel with a coefficient of thermal expansion of 17.3×10^{-6} to the 400°C bakeout temperature. It was assumed that a maximum temperature difference of 100°C between the baffle and the vessel floor can be controlled during bakeout. The differential radial thermal growth between the baffle and the vessel floor for the assumed temperature difference of 100°C is 7.0 mm. The initial sizing calculations indicated that Inconel 718 material with a yield stress of 1035 MPa to 400°C would be required for the flexible plate concepts. Sizing calculations for the maximum thickness of the supports are based on a clamped-clamped beam model with the imposed thermal displacement. The allowable thermally induced stress (elastically calculated) for the Inconel 718 is based on the material ultimate strength of 1242 MPa. The selected plate thickness of 1.9 cm results in a maximum bending stress of 1118 MPa for the assumed bakeout condition.

The calculated halo current loads are based on a nominal halo current of 0.45 I_p with a toroidal peaking factor of 2.0. An assumed halo current flow path in the private flux baffle and its supports is shown in Fig. 5. The peak halo current in a support plate can be as high as 200 kA. This current crossing a toroidal field of 7.14 T at the baffle produces a distributed load of 1428 kN/m (8154 lb/in.). A support plate width of 20.3 cm was selected to assist in reacting the resultant side load developed from the halo current loads

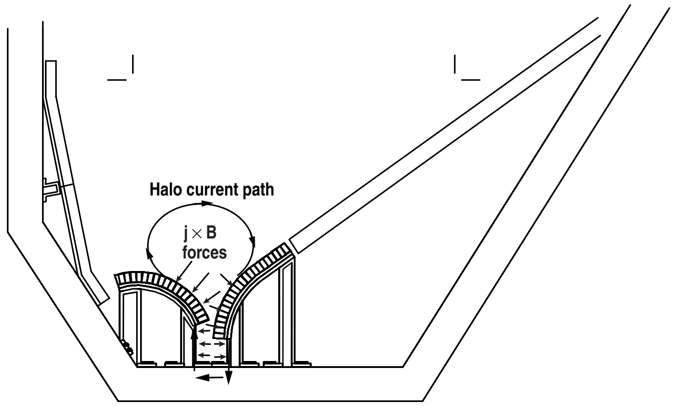

Fig. 5. Assumed halo current path. The peak halo current can be 200 kA in a single support plate producing a distributed load of 1428 kN/m.

with a 2:1 peaking factor. The total divertor plate segment width is about 60 cm, so the support plate will block only about one-third of the path for neutral pumping. The toroidal distribution of the halo current pressure on the outer half of the dome structure (Fig. 5) is calculated to be:

$$P = 7140\,(1 + \cos\theta)\ \mathrm{N/cm} \quad .$$

Initial sizing of the support plates for the baffle structure using a clamped-clamped beam model showed that a 1.9 × 20.3 cm plate is adequate for reacting the peak halo current load. However, the toroidally continuous structure does not provide a clamped end boundary condition due to its flexibility. Therefore, the 180-deg finite element model of the baffle and its supports was developed to more accurately calculate the maximum stress and displacement of the support plates. The model consists of 3–D beam and shell elements input to the COSMOS finite element code [15]. The thickness of the shell elements was sized to be 3.0 cm to maintain bending stresses between supports to be less than 241 MPa. The same structural model was also used to verify hand calculations for the thermally induced stresses during the assumed bakeout condition.

The analytical results from the finite element model showed that two supports, 1.9 × 20.3 cm and spaced at 8°, are required at each end of the private flux baffle to react the halo current loads. The supports are closely spaced providing an equal splitting of the halo current between the two. The deformed shape of the dome structure and its supports is shown in Fig. 6. A maximum displacement of 3.6 mm occurs in the dome structure between the supports where the maximum halo current forces exist. The maximum stress intensity in the private flux baffle is 222.7 MPa. This is less than the 241 MPa yield stress for 316 LN stainless steel. The maximum displacement at the support end which attaches to the baffle structure is 2.9 mm. The maximum displacements can be greatly reduced by incorporating horizontal struts connecting the ends of the baffle. The maximum stress in the supports is 818 MPa, less than the 1035 MPa yield stress for Inconel 718.

The finite element model was also used to analyze the bakeout condition in which the vessel floor is 100°C hotter than the private flux baffle. The results show that the maximum stress in the structure between support points is 272 MPa. The allowable thermal stress for 316 LN at 400°C is 327 MPa. The maximum stress in the supports for bakeout is 614 MPa. This is less than the yield stress of 1035 MPa for Inconel 718 at 400°C. It is concluded that the proposed double-flexible plate support concept is acceptable for reacting the halo current loads and bakeout conditions without exceeding the yield stress of the selected materials.

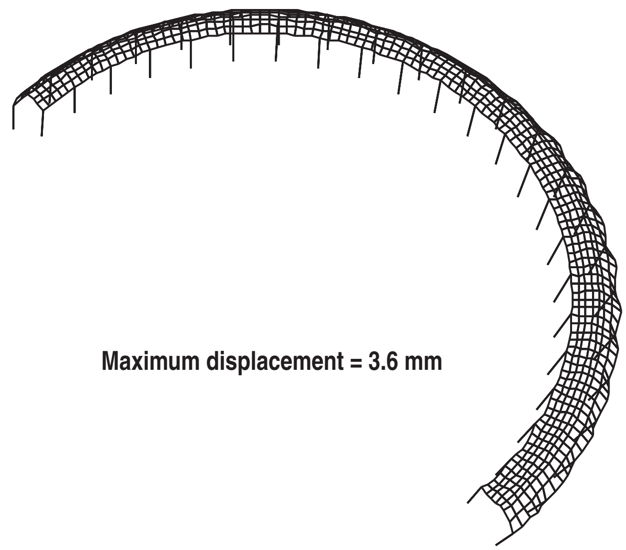

Fig. 6. Deformed shape of divertor due to halo current loads.

Simple estimates were made to size the longest support (66 cm) for the outer baffle structure. It was assumed that the clamped-clamped beam model is an adequate model for the stiffer outer baffle structure. The peak distributed halo current load on the outer support was calculated to be 1220 kN/m. Assuming a plate width of 20.3 cm, the required thickness of Inconel 718 plate is 4.45 cm. In order to accommodate a differential thermal growth of 8.5 mm between the ends of the support plates, two 1.9 × 20.3 cm plates with a length of 25 cm are used to join the large plates as shown in Fig. 7. The smaller plates are positioned near the top end of the support where the bending moment due to halo current load changes from positive to negative values. Verification of the sizing calculations was made using a finite element model of a clamped-clamped beam with discontinuous section properties. The calculated maximum stress in the support post is 849 MPa due to the peak halo current load and 417 MPa for the bakeout condition. The stress criteria are, therefore, satisfied by this long support concept.

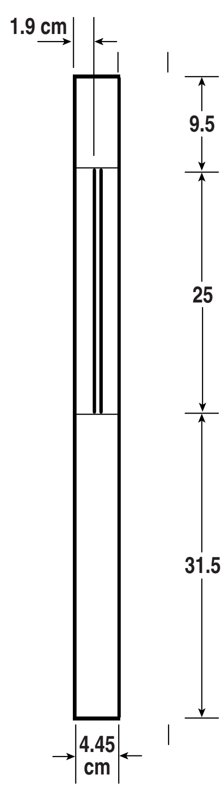

Fig. 7. Cross section of the long (66 cm) strut needed to support the outboard side of the outer baffle. The material is Inconel 718.

4. DIVERTOR TILE HEAT FLUX AND COOLING

One of the important factors in the definition of the geometry of the divertor was the reduction of the peak heat flux on the divertor. This section examines the heat flux for the new JT–60SU DN plasma configuration and the associated surface temperature of the carbon fiber composite (CFC) tiles. Heat flux to the lower divertor for lower SN operation using the proposed divertor baffle design will also be examined. The desired peak temperature of the surface of the tile is 1200°C, which is set by the durability and erosion rate of the CFC plasma-facing tiles. A conceptual design is presented which integrates the tile geometry into the baffle segment.

4.1. AN ASSESSMENT OF HEAT FLUX IN THE JT–60SU DIVERTOR

4.1.1. Estimating Peak Heat Flux

The peak heat flux on the divertor surfaces is estimated by assuming that the radial heat flux distribution is toroidally symmetric and has an exponential form, *i.e.*,

$$Q_{div} = Q_{div,0} \times exp\left[-\frac{\left(R - R_S\right)}{f_{exp} \times \lambda_p}\right] \quad , \tag{1}$$

where Q_{div} is the radial heat flux distribution, $Q_{div,0}$ is the peak heat flux at the divertor strike point, R_S is the major radius of the divertor strike point, R is restricted to $\geq R_S$, λ_p is the midplane heat flux scrapeoff length, and f_{exp} is the flux expansion at the divertor target. The total amount of power P_{div} that flows into a divertor can be written as:

$$P_{div} \approx P_{input} \times (1 - f_{rad}) \times f_{outboard}/\mathrm{total} \times f_{grad–B}/\mathrm{total} \times (1 - f_{pfr}) \quad , \tag{2}$$

where P_{input} is the total input power, f_{rad} is the ratio of total radiated power to total input power, $f_{outboard}$/total is the ratio of power flowing into the outboard scrapeoff layer (SOL) to the power flowing into both inboard and outboard SOL, $f_{grad–B}$/total is the ratio of power striking the outboard divertor in the grad–B direction to the power striking both upper and lower outboard divertors, and f_{pfr} is the fraction of power flowing into the private flux region.

$$Q_{div,0} = \frac{P_{input} \times \left(1 - f_{rad}\right) \times f_{outboard/total} \times f_{grad-B/total} \times \left(1 - f_{pfr}\right) \times \sin(\alpha)}{2\pi x R_s \, f_{exp} \times \lambda_p \times \left(1 + \dfrac{f_{exp} \times \lambda_p}{R_s}\right)} \quad , \quad (3)$$

where α is the angle between the divertor incline and the separatrix. For estimating the peak heat flux in this study, we use the parameter values shown in Table 3, which are based on the lower divertor geometry shown in Fig. 2. Two main operational configurations considered here are the lower single-null (with the grad–B particle drift toward that divertor) and the magnetically balanced double null.

TABLE 3
PARAMETERS OF SINGLE-NULL AND DOUBLE-NULL CASES

	Single Null	Double Null
λ_p	0.01	0.01
$R_{s–inboard}$ (m)	3.5	3.5
$R_{s–outboard}$ (m)	4.3	4.3
α (m) — inboard	85°	85°
α (m) — outboard	45°	45°
$f_{inboard/total}$	0.33	0.17
$f_{outboard/total}$	0.67	0.83
f_{exp}	7	7
f_{pfr}	0.1	0.1
$f_{grad–B/total}$ — lower divertor	1.0	0.6
$f_{grad–B/total}$ — upper divertor	—	0.4

4.1.2. Power Flow and Peak Heat Flux to the Divertor Components

With Eq. (2), we estimate the power flow onto the inner and outer plasma-facing divertor components. Analyses of SN and DN DIII–D plasmas indicate that approximately 10% of the power flow to the divertors is transported across the separatrix into the private flux region. In the standard positioning of the inner and outer strike points (Fig. 2), this will likely heat the private flux baffle. Note that running the divertor strike points on the private flux baffle itself is an option which would significantly complicate the cooling requirements of the baffle (see Section 4.1). Tables 4 and 5 summarize the results in terms of the given fraction of power input that is radiated away. A fixed total power input of 80 MW is assumed.

TABLE 4
THE POWER FLOWS TO THE INBOARD AND OUTBOARD DIVERTORS ARE SHOWN AS A FUNCTION OF RADIATED POWER IN THE CORE PLASMA. FOR THE DN CASE, TWO DIVERTOR POWER FLOW VALUES ARE LISTED, TOWARD (AWAY FROM) THE ∇B DIRECTION.

		Single Null		Double Null	
f_{rad}	P_{rad} (MW)	$P_{div,inner}$ (MW)	$P_{div,outer}$ (MW)	$P_{div,inner}$ (MW)	$P_{div,outer}$ (MW)
0.00	0	24.0	48.0	7.2 (4.8)	36.0 (24.0)
0.25	20	18.0	36.0	5.4 (3.6)	27.0 (18.0)
0.50	40	12.0	24.0	3.6 (2.4)	18.0 (12.0)
0.75	60	6.0	12.0	1.8 (1.2)	9.0 (6.0)
1.00	80	0.0	0.0	0.0 (0.0)	0.0 (0.0)

In Tables 4 and 5 the DN columns contain two entries. Data from present day experiments indicate that for a magnetically balanced DN, the power flow to the divertor in the direction of ∇B may be between 1.0 and 1.5 times that of the other divertor. The two quantities shown represent the heat flux to the ∇B (away from ∇B) divertors.

TABLE 5
THE PEAK HEAT FLUX AT INBOARD AND OUTBOARD STRIKE POINTS IS SHOWN AS A FUNCTION OF RADIATED POWER IN THE CORE PLASMA. FOR THE DN CASE, TWO DIVERTOR POWER FLUXES ARE LISTED, TOWARD (AWAY FROM) THE ∇B DIRECTION.

		Single Null		Double Null	
f_{rad}	P_{rad} (MW)	$Q_{0,inner}$ (MW/m^2)	$Q_{0,outer}$ (MW/m^2)	$Q_{0,inner}$ (MW/m^2)	$Q_{0,outer}$ (MW/m^2)
0.00	0	15.6	18.0	4.8 (3.2)	13.4 (9.0)
0.25	20	11.7	13.5	3.6 (2.4)	10.0 (6.8)
0.50	40	7.8	9.0	2.4 (1.6)	6.7 (4.5)
0.75	60	3.9	4.5	1.2 (0.8)	3.4 (2.3)
1.00	80	0.0	0.0	0.0 (0.0)	0.0 (0.0)

4.1.3. Excessive Heat Load Conditions

When the inner and outer strike points of the divertors are located properly, the power flow and the peak heat flux appear manageable under probable operating conditions. However, if the strike point locations are not well controlled and are allowed to “wander,” then one must be concerned about excessive heating of regions of the vessel not properly “armored.” Some examples are given below.

For the SN divertor, the outer strike point may move onto the top of the lower private flux baffle. When this happens, the baffle receives considerable power, ≈14 MW/m^2 (again, assuming f_{rad} = 0.5).

If the outer strike point moves away from its standard slot location and farther up onto the outboard baffle, local heating can again be relatively high as the angle α approaches 90 deg. In this case, the peak heat flux could be ≈12 MW/m^2 where f_{rad} = 0.5 and power input is 80 MW.

A similar situation exists in the upper divertor, which is assumed to be the mirror of the lower divertor. Although a balanced DN configuration will result in most of the power flow going to the lower divertor, even a modest bias of the DN toward the upper divertor may result in a shift of ~80% of the power flow into the upper divertor. In operating the magnetically balanced DN, either shape control must be very reliable or the upper divertor should expect occasional heat loading comparable to that of the lower divertor.

4.2. THERMAL ANALYSIS OF JT–60SU DIVERTOR

The power flows and peak heat fluxes expected on JT–60SU divertor [16] are shown in Tables 4 and 5 of Section 4.1. The divertor is assumed to be divided toroidally into 45 modules. The thermal design of the divertor is based on the following assumptions: input power = 80 MW, radiated power fraction = 50%, the maximum allowable surface temperature of divertor = 1200°C, maximum coolant temperature = 100°C, inlet coolant pressure = 3 MPa, the coolant tube inside diameter = 15 mm, individual tile width = 30 mm.

Using a CFC with properties shown in Table 6 as a plasma-facing material [16] and a peak heat flux of 9 MW/m^2 at 50% radiated power fraction (Table 5), the peak surface temperature is calculated to be about 1200°C if a coolant velocity of 1.7 m/s is maintained. The safety margin on critical heat flux will be about 2.

TABLE 6
THERMAL CONDUCTIVITY OF CFC TILES

Temperature (°C)	Thermal Conductivity (‖ to Plasma-Facing Side) (W/cm-C)	Thermal Conductivity (⊥ to Plasma-Facing Side) (W/cm-C)
0	0.35	5.7
500	0.2	3
1000	0.15	2.5

Each outer divertor module is about 61 cm in toroidal direction and about 60 cm in the poloidal direction. We will assume that the coolant channels are poloidal in direction. The coolant channel is brazed into a copper saddle block about 3 cm wide that runs the poloidal extent of each of the three baffles. Graphite (CFC) tiles about 3 cm square are brazed onto the top of the blocks and serve as the plasma-facing material. A cross section of a saddle block with coolant channel and brazed CFC tile is shown in Fig. 8. The flow path in each block is into the lower channel and out from the upper channel. A swirl tape insert is used in the flow channels to enhance the heat transfer. Within a baffle module, the flow through the approximately 20 blocks will be in parallel. The inlet pressure is assumed to be 3 MPa so that a subcooling of 100°C is available at the exit. This is required for adequate margin on critical heat flux. The inlet coolant temperature should be less than 50°C.

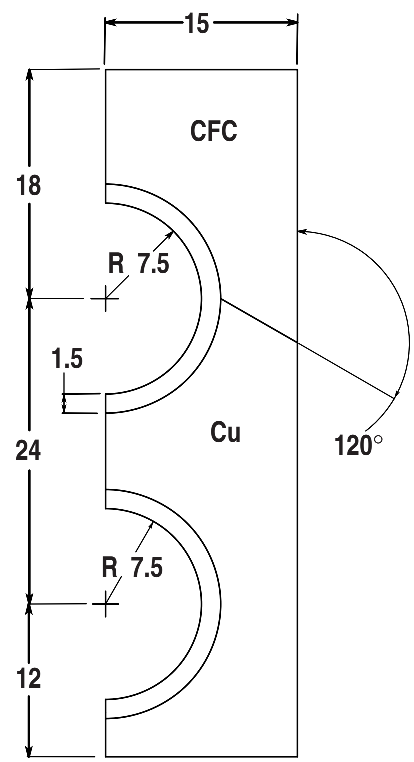

Fig. 8. Cross section of the actively cooled tiles for the JT–60SU divertor plates (mm).

The required flow velocity in the coolant channels is calculated based on the critical heat flux (CHF). Using a safety factor of two in the CHF, an incident heat flux at the plasma-facing surface of 9 MW/m^2 (from Table 5, SN case at 50% radiation factor) and an incident-to-channel heat flux ratio of 1.2 (calculated using the ANSYS finite element thermal transport code [17]), a CHF of 21.5 MW/m^2 is estimated. The poloidal extent of this high heat flux region on the outer baffle is only about 5 cm, so a coolant flow velocity of only 1.7 m/s is estimated to be adequate. The total flow rate to the divertor will be 775 ℓ/s.

4.3. DESIGN OF BAFFLE COOLING BLOCKS

A preliminary conceptual design that integrates the slantblock cross section of Fig. 8 with the divertor geometry and hardware is shown in Fig. 9. Details of the mounting scheme of the baffle segment to the splice plate as well as the interfaces to the cooling manifold have not been finalized. These design details await further work.

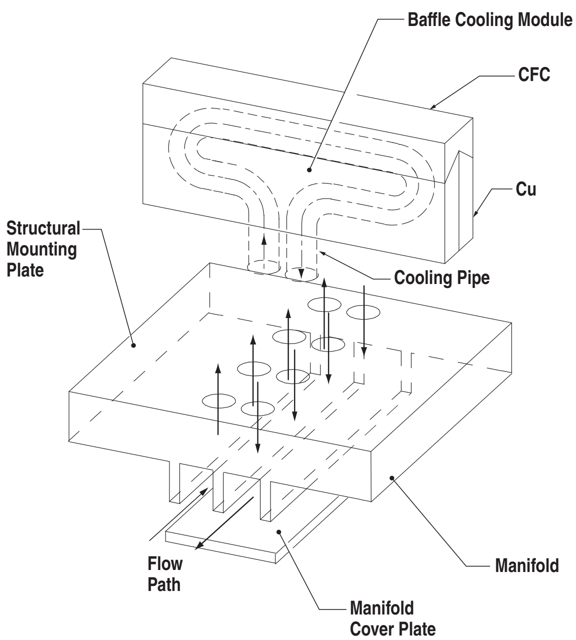

Fig. 9. Schematic of the divertor cooling module with the divertor mounting plate and the cooling water manifold.

The main components of this design are the baffle cooling block and the structural mounting plate. The baffle cooling block is based on the slantblock cross section which is essentially two cooling lines imbedded in a copper block to which the CFC material is brazed. For this design, the copper blocks are machined in halves to allow for machining of grooves to hold the copper cooling pipes. After the preformed pipes are inserted in the grooves, the two halves are joined, perhaps mechanically, together. The pipes extend past the copper blocks to allow for interfacing with the structural mounting plate. Once the baffle cooling modules are assembled, they are bolted to the mounting plate. The cool ing pipes extend through the mounting plate and into the cooling manifold. Welding access is from the backside of the mounting plate prior to the welding of the manifold cover plate. Each manifold, in turn, is connected to either an inlet or outlet line. Flow through the modules is thus in parallel and runs in the poloidal direction.

5. DIVERTOR GAS CONDUCTANCE AND THROUGHPUT

The divertor baffles should simultaneously provide good shielding of the recycling neutrals from reentering the main plasma directly through the SOL while allowing good conductance of the gas from the strike zones to the ex-vessel exhaust pumps. For advanced divertor operation in a strongly radiating plasma, it is likely that forced SOL flow using the “puff and pump” technique [18] will be used. In a steady-state condition, this mode will provide the largest gas throughput in the divertor so we have chosen to analyze the divertor pumping performance under these conditions. The required gas throughput for the “puff and pump” operating mode is scaled from DIII–D SN divertor data. On DIII–D, a total D_2 throughput of 20 Pa m^3/s has been observed to provide significant enrichment of the concentration of trace levels of argon impurity in the divertor. To scale to JT–60SU, we assume that an equivalent flow rate of D^+ in the SOL will provide good enrichment of an injected impurity in the divertor. We also assume that in high confinement modes, the SOL width is independent of the size of the tokamak. With these assumptions, the required gas throughput will scale as the major radius of the tokamak so on JT–60SU we anticipate a total gas throughput of 50 Pa m3/s. The conductance of the gaps in the divertor baffles is obtained from the simple formula for the conductance of an aperture, corrected for the finite thickness of gap using Monte Carlo models:

$$C\ (\mathrm{m3/s}) \;=\; 1.16 \times 10^5\, \alpha\, A\ (\mathrm{m}^2) \quad .$$

Where A is the area of the aperture and α is the correction factor obtained from Fig. 2.9 in O’Hanlon [19]. The total pumping speed of the ex-vessel turbo-molecular exhaust pumps was obtained from a communication from A. Sakasai [20] as was the conductance of the pumping ducts. Using this simple model, the pressure under the outer baffle is calculated to be 1.4 Pa. Because of the large conductance of the gap between the private/outer baffles and the machine floor, the pressure under the private flux baffle is 1.5 Pa. Such divertor pressures are typical during highly radiative operation.

6. SUMMARY

An up/down symmetric DN divertor design for highly triangular elongated DN plasma operation on JT–60SU is described. A tightly baffled arrangement is produced using contoured plasma-facing surfaces. The divertor shape was designed to fit equilibria produced using the EFIT-free boundary equilibrium solver. These equilibria are consistent with approximate flux states expected at start of flattop and at the end of burn. Estimated D_2 conductance is shown to be consistent with requirements for active control of impurities using the puff and pump technique.

A simplified component mounting scheme was adopted to the new DN JT–60SU divertor geometry and halo current loads. This design avoids the use of insulators and sliding block mechanisms in the interest of improving divertor reliability and maintainability. Remote maintenance accessibility was also a consideration in the development of this design.

Simulations show that JT–60SU can produce a peak axisymmetric halo current fraction $I_{h(pol)}/I_{p0}$ ~ 0.47 in the case of a post-thermal quench core and halo temperature of 25 eV for an equilibrium with initial growth rate of γ_z = 50 s^{-1}.

New stress analyses of support concepts for the proposed JT–60SU divertor were performed for an assumed bakeout condition and the calculated halo current loads. The purpose of the analyses was to evaluate the utilization of supports that are flexible to allow for differential thermal displacements between the toroidally continuous divertor structures and the vacuum vessel, but also be sufficiently stiff to react the peak halo current loads. The results show that flexible plates fabricated from Inconel 718 will provide a reasonable support concept for the divertor baffle structures.

Under normal operation with the divertor described in this report, the peak flux in the divertors appears manageable. This may relax the need for dramatic divertor plasma and/or edge cooling (and the accompanying risk of adversely affecting the high performance core plasma). Still, care must be taken to avoid “nonstandard” configurations, which may generate excessively high heat loads in relatively unprotected regions of the vessel. In future work, it is important to make a closer examination of such “unanticipated” situations.

A thermal analysis of the JT–60SU divertor was performed. The power flows and heat fluxes were based on the assumption that the input power is 80 MW and 50% of this power is radiated. A slantblock design with a block width of 30 mm and a flow channel diameter of 15 mm was used in this analysis. Based on the heat fluxes and geometry, a flow velocity of 1.7 m/s was found to be sufficient to keep the surface temperature of the CFC below 1000°C and to provide a safety factor of 2 for the critical heat flux. The total flow required is 775 ℓ/s. The pressure drop will be <0.5 MPa. Details of the mechanical design of the cooling water manifolds and their integration with the mounting plates awaits further work.

The conceptual design presented here is intended for the deuterium operation phase of the JT–60SU program. The analysis indicates that this symmetric DN design can readily handle the estimated mechanical loads, and the thermal loads are tolerable even during the more stressful SN operation. The design is based on well-documented studies of the physics of the tokamak divertor as well as halo current generation during tokamak disruptions. Self-heating arising from the tritium operation, as well as plasma materials interaction issues and structural materials activation issues, have not been addressed in this design. However, improvements in this design needed to address these issues can be most efficiently integrated after operation experience during the deuterium phase.

7. REFERENCES

[1] Lao, L., *et al.* , Nucl. Fusion **30** (1990) 1035.

[2] Nakamura, Y., *et al.*, Nucl. Fusion **36** (1996) 643.

[3] Yoshino, R., Nakamura, Y., Neyatani, Y., Nucl. Fusion **36** (1996) 295.

[4] Kikuchi, M., *et al.*, "Design Progress of JT-60SU," Proc. 16th Int. Conf. on Plasma Physics and Controlled Nuclear Fusion Research, Montreal, Canada, Vol. 3, p. 451 (International Atomic Energy Agency, Vienna, 1997).

[5] Kurita, G., *et al.*, "Present Status of JT-60SU Design," Proc. 17th IEEE/NPS Symp. on Fusion Engineering, San Diego, California, Vol. 1, p. 223 (Institute of Electrical and Electronics Engineers, Inc., Piscataway, New Jersey, 1998).

[6] Allen, S., *et al.*, "Radiative Divertor and SOL Experiments in Open and Baffled Divertors on DIII–D," presented at 17th IAEA Fusion Energy Conf., October 19–24, 1998, Yokohama, Japan, to be published in a special issue of Nucl. Fusion; General Atomics Report GA–A23004 (1998).

[7] Strait, E.J., *et al.*, Nucl. Fusion **31** (1991) 527.

[8] Granetz, R.S., *et al.*, Nucl. Fusion **36** (1996) 545.

[9] Evans, T.E., *et al.*, J. Nucl. Mater. **241–243** (1997) 606.

[10] Humphreys, D.A., Kellman, A.G., Phys. Plasmas **6** (1999) 2742.

[11] Humphreys, D.A., *et al.*, "Analytic Halo Current Models Applied to Disruptions in Present and Next-Generation Tokamaks," Bull. Am. Phys. Soc. **43** (1998) 1875.

[12] Humphreys, D.A., *et al.*, Phys. of Plasmas **6** (1999) 2742.

[13] Humphreys, D.A., *et al.*, "Scoping Studies of ITER Disruption Scenarios Using the DINA Code," Contribution to U.S. Disruption Physics R&D Report for FY97, ITER/US/97/PH-14 (1997).

[14] Kurita, G., *et al.*, Fusion Engineering and Design **38** (1998) 417.

[15] COSMOS/M, a self-contained finite element structural analysis code available from Structural Research Analysis Corporation, Los Angeles, California.

[16] Neyatani, Y., *et al.*, “The Design Study of JT–60SU Device (No. 4) — The Vacuum Vessel and Cryostat of JT–60SU,” Japan Atomic Energy Research Institute, JAERI-Research 97-024 (1997).

[17] ANSYS, a finite element thermal analysis code available from Swanson Analysis Systems, Inc., Houston, Pennsylvania.

[18] Wade, M.R., *et al*., Nucl. Fusion **38** (1998) 1839.

[19] O’Hanlon, J.F., *A User’s Guide to Vacuum Technology*, (John Wiley & Sons, New York, 1980).

[20] Sakasai, A., private communication, March 10, 1999.